*Acta of Bioengineering and Biomechanics*
*Vol. 13, No. 1, 2011*

Original paper

# Analysis of wall shear stress around a competitive swimmer using 3D Navier–Stokes equations in CFD

C.V. POPA[a]*, H. ZAIDI[a], A. ARFAOUI[a], G. POLIDORI[a], R. TAIAR[b], S. FOHANNO[a]

[a] GRESPI/Thermomécanique, Université de Reims Champagne-Ardenne, Reims, France.
[b] Laboratoire d'Analyse des Contraintes Mécaniques, Université de Reims Champagne-Ardenne, Reims, France.

This paper deals with the flow dynamics around a competitive swimmer during underwater glide phases occurring at the start and at every turn. The influence of the head position, namely lifted up, aligned and lowered, on the wall shear stress and the static pressure distributions is analyzed. The problem is considered as 3D and in steady hydrodynamic state. Three velocities (1.4 m/s, 2.2 m/s and 3.1 m/s) that correspond to inter-regional, national and international swimming levels are studied. The flow around the swimmer is assumed turbulent. The Reynolds-averaged Navier–Stokes (RANS) equations are solved with the standard $k$–$\omega$ turbulent model by using the CFD (computational fluid dynamics) numerical method based on a volume control approach. Numerical simulations are carried out with the ANSYS FLUENT® CFD code. The results show that the wall shear stress increases with the velocity and consequently the drag force opposing the movement of the swimmer increases as well. Also, high wall shear stresses are observed in the areas where the body shape, globally rigid in form, presents complex surface geometries such as the head, shoulders, buttocks, heel and chest.

*Key words*: *swimmer, wall shear stress, static pressure, standard k–ω turbulence model, CFD*

## 1. Introduction

The glide phase, which plays a significant role during swimming starts and turns, is one of the most important elements in swimming races as it allows the wave drag effects to be avoided. It is the reason why the FINA rules impose a 15 m limit on underwater swimming phases. The hydrodynamic performance in swimming depends greatly on the technique adopted by the swimmers during the different phases of swimming as well as on the drag force opposing their movements in water. Moreover, it is known (NAEMI et al. [14], BIXLER and RIEWALD [10]) that the drag force greatly depends on pressure and wall shear stress fields around the swimmer. So, improving the performance requires a better understanding of the flow behaviour around swimmers (pressure field and wall shear stress distribution) in order to minimize the drag force.

Several authors carried out measurements of the drag acting on the whole body of the swimmer and estimated the influence of various parameters such as the swimmer's position, morphology or velocity on the intensity of the drag ([1]–[5]). In the biomechanics of swimming, concerning both fishes and human swimmers, the computational fluid dynamics (CFD) has been extensively used for last years due to the complexity of the experiments and the development of computers (ADKINS and YAN [6], KATO et al. [7], SATO and HINO [8], MARINHO et al. [9]). BIXLER and RIEWALD [10] first used the CFD method to simulate the water flow around a swimmer's hand and forearm. The aim of their study was to calculate the drag forces and their coefficients around a swimmer's hand and forearm in the case of different angles of attack. ROUBOA et al. [11] estimated numerically the drag and lift coefficients for a swimmer's hand and forearm in both the steady and unsteady state cases. They also

* Corresponding author: C.V. Popa, GRESPI/Thermomécanique, Université de Reims Champagne-Ardenne, Moulin de la Housse, BP 1039, 51687 Reims, France. Tel. +33326913278. E-mail: catalin.popa@univ-reims.fr
Received: June 26th, 2010
Accepted for publication: January 9th, 2011

evaluated the effect of the acceleration of the hand and forearm on the generation of the propulsive force. GARDANO and DABNICHKI [12] performed numerical simulations in order to highlight the importance of the analysis of flow around the whole arm of a swimmer, so that the exact values of the propulsion and the drag forces were estimated. BIXLER et al. [13] used the CFD method to estimate the drag forces encountered by the swimmer during the underwater glide phase and to study the effect of wearing a wetsuit on the drag forces. More recently, the numerical results obtained by ZAÏDI et al. [15] in a 2D geometry case revealed that the position of the head had a noticeable effect on the hydrodynamic performances in underwater phase of start and turn. The analysis of these results made it possible to propose an optimal position of the swimmer's head in underwater glide swimming. Five turbulence models were tested by ZAÏDI et al. [16] in a 2D configuration and steady hydrodynamic state. The comparison between these models and experimental results reveals that the standard $k$–$\omega$ turbulence model is the most appropriate to predict the flow around the swimmer. More recently, ZAÏDI et al. [17] studied a 3D geometry using a CFD code. Two turbulence models were tested, namely the standard $k$–$\varepsilon$ turbulence model and the standard $k$–$\omega$ turbulence one, in order to predict drag forces during the underwater glide phases. The comparison between numerical results and experimental measurements of drag forces shows that the standard $k$–$\omega$ model accurately predicts the drag forces while the standard $k$–$\varepsilon$ model underestimates their values. By making the assumption that the swimmer can adopt a rigid posture of the body, it can be expected that in a laminar turbulent transition $Re$ approaches $5\times10^5$. This implies that the flow around the swimmer is mainly turbulent [17]–[20].

The objective of this paper was to study the flow dynamics around the swimmer during underwater glide phases in swimming. Three velocities ($U_0$ = 1.4, 2.2 and 3.1 m/s) corresponding to the following range of the Reynolds number $4\times10^6 \le Re \le 9\times10^6$ (ZAÏDI et al. [16]) were studied. These values correspond to the velocity at the time of the departure (underwater glide phase after start dive) from inter-regional, national and international swimming levels (TOUSSAINT et al. [3]). Also, the influence of the head position, namely lifted up, aligned and lowered, on the wall shear stress and static pressure distributions were analyzed. To the authors' knowledge, this study is the first investigation of the pressure field and wall shear stress distribution around the whole swimmer's body. Three glide positions were investigated, depending on whether the head is aligned with the body, lifted up or lowered.

# 2. Material and methods

## 2.1. Geometry and mesh

The construction of the 3D geometric model of the swimmer follows the same procedure as that described by ZAÏDI et al. [17]. The subject chosen for the present study is a national-level male swimmer. The equipment used in the construction of his 3D geometric model is a Konica Minolta® scanner, which is commanded by a laser scanning process. The scanner allows the creation of data files containing all the coordinates of all the points defining the layer on the surface of the swimmer's body. The RapidForm® software has been used in the construction of the swimmer's geometry using the data file that contains the clouds of points coming from the scanner.

Then, the geometry of the swimmer was constructed starting with the simplest parts (legs, arms and trunk) and continued with the more complex parts (head, feet, hands and pelvis). After constructing all parts of the swimmer, the next step consists in putting them together to build the final geometric envelope (figure 1). The length of the swimmer with arms and hands outstretched corresponds to the glide position of the swimmer in the underwater starting phase. This measured length is 2.4 m. In this study, three glide positions were maintained, differing only in the head position, namely lifted up, aligned and lowered corresponding to positions 1, 2 and 3 schematized in figure 2.

Fig. 1. Swimmer's model after reconstruction

After constructing the swimmer's geometry, the next step is to build the fluid domain around his body. The size of the fluid domain was chosen by referring to the study by ZAÏDI et al. [17]. Figure 3 shows the dimensions of the fluid domain built around the swimmer.

The mesh of the fluid around the swimmer was created using the Gambit® and the TGrid® softwares. It consists of a progressive three-dimensional mesh refined near the surface of the swimmer (to identify the strong gradients of physical quantities) and rough when it is far (to avoid burdening with the computation time). The surface of the swimmer and the surfaces limiting the fluid domain are meshed using triangular cells. However, tetrahedral cells are used for

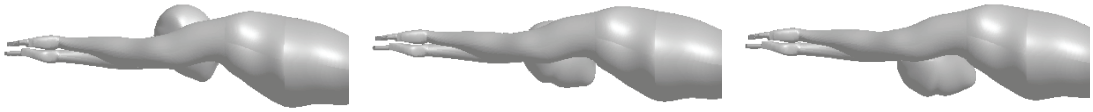

a) lifted up b) aligned c) lowered

Fig. 2. Three head positions maintained in the study

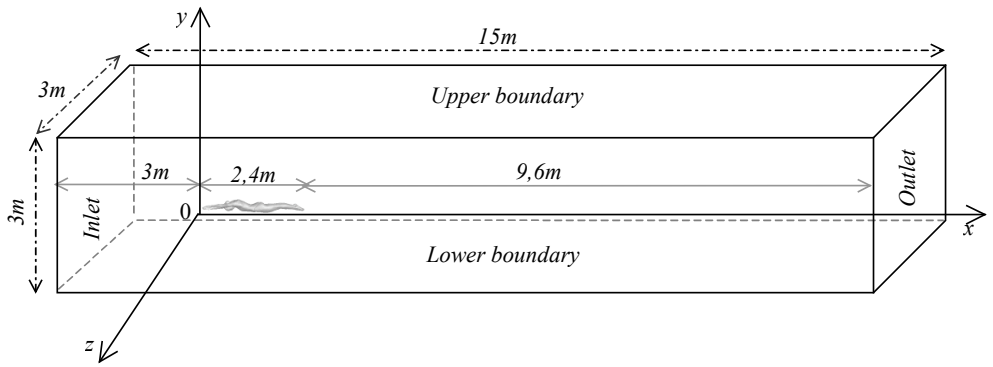


Fig. 3. Fluid domain built around the swimmer

meshing the fluid domain. The total number of cells are about 2 billion, and the sensitivity of the mesh has been previously studied (ZAÏDI et al. [17]).

The boundary conditions chosen in this study are the following:

- At the inlet of the fluid domain: a uniform velocity profile $U_0$ = 1.4, 2.2 and 3.1 m/s.
- At the outlet of the fluid domain: all gradients are null.
- On the upper, lower, left and right borders of the fluid domain: the symmetry condition is imposed.
- On the surface of the swimmer: the no-slip condition is imposed.

## 2.2. Mathematical formulation

The flow around the swimmer is assumed to be fully turbulent [5], [15]–[18]. Such a flow is governed by the Reynolds-averaged Navier–Stokes (RANS) equations. These equations are obtained by introducing the Reynolds decomposition, which consists in considering that in turbulent flows each instantaneous variable is the sum of a mean component and a fluctuating component. Then, the time-averaging of the instantaneous equations leads to the following system of averaged equations (ZAÏDI et al. [17]):

- Continuity equation

$$\frac{\partial}{\partial x_i}(\overline{U}_j) = 0\,. \tag{1}$$

- Navier–Stokes equations

$$\frac{\partial}{\partial x_j}(\rho \overline{U}_i \overline{U}_j) = \frac{\partial \overline{p}}{\partial x_i} + \frac{\partial}{\partial x_j}\left[\mu\left(\frac{\partial \overline{U}_i}{\partial x_j} + \frac{\partial \overline{U}_j}{\partial x_i}\right) - \rho \overline{u}_i \overline{u}_j\right], \tag{2}$$

where:

$\overline{U}_i(t) \equiv \overline{U}_i + u_i$ – the instantaneous velocity component in the i direction (m/s),

$\overline{U}_i$ – the mean (time-averaged) velocity component in the $i$ direction (m/s),

$u_i$ – the fluctuating velocity component in the $i$ direction (m/s),

$i, j$ – the directions,

$\rho$ – the fluid density (kg/m$^3$)

$\mu$ – fluid dynamic viscosity (kg/ms).

In the Reynolds-averaged Navier–Stokes approach to turbulence modelling, the Reynolds stresses ought to be appropriately modelled. A common method employs the Boussinesq hypothesis to relate the Reynolds stresses $(-\rho \overline{u}_i \overline{u}_j)$ to the mean velocity gradients:

$$-\rho \overline{u}_i \overline{u}_j = \mu_t\left(\frac{\partial \overline{U}_i}{\partial x_j} + \frac{\partial \overline{U}_j}{\partial x_i}\right) - \frac{2}{3}\delta_{ij}\rho k\,, \tag{3}$$

where the Kronecker symbol is $\delta_{ij} = 1$ if $i = j$ and $\delta_{ij} = 0$ if $i \neq j$.

The turbulent viscosity is not a property of the fluid itself but depends on the dynamic characteristics of the turbulent flow. In this paper, the turbulent vis-

cosity is modelled by means of the first-order models based on the time-averaged dynamical characteristics of the turbulent flow. The standard $k$–$\omega$ model was chosen because it is well suited to wall-bounded flows like the flow around the body contour of the swimmer (ZAÏDI et al. [17]). The standard $k$–$\omega$ turbulence model is an empirical model based on transport equations for the turbulent kinetic energy per unit mass ($k$) and the specific dissipation rate ($\omega$). Two additional transport equations for the turbulent kinetic energy per unit mass ($k$) and the specific dissipation rate ($\omega$) are solved. These equations are:

$$\frac{\partial}{\partial x_j}(\rho k \overline{U}_j) = \frac{\partial}{\partial x_j}\left(\Gamma_k \frac{\partial k}{\partial x_j}\right) + P_k - Y_k, \tag{4}$$

$$\frac{\partial}{\partial x_j}(\rho \omega \overline{U}_j) = \frac{\partial}{\partial x_j}\left(\Gamma_\omega \frac{\partial \omega}{\partial x_j}\right) + P_\omega - Y_\omega, \tag{5}$$

where $Y_k$ and $Y_\omega$ are the turbulent dissipations of $k$ and $\omega$, respectively.

The effective diffusivities for $k$ and $\omega$ are given by:

$$\Gamma_k = \mu \frac{\mu_t}{\sigma_k}, \tag{6}$$

$$\Gamma_\omega = \mu \frac{\mu_t}{\sigma_\omega}, \tag{7}$$

where $\sigma_k$ and $\sigma_\omega$ are the turbulent Prandtl numbers for $k$ and $\omega$, respectively.

The turbulent viscosity ($\mu_t$) is then calculated as the function of $k$ and $\omega$:

$$\mu_t = \alpha^* \frac{\rho k}{\omega}, \tag{8}$$

where $\alpha^*$ is the coefficient allowing us to correct the turbulent viscosity at low Reynolds numbers.

The production of $k$ and $\omega$ due to mean velocity gradients are:

$$P_k = -\rho \overline{u}_i \overline{u}_j \frac{\partial \overline{U}_j}{\partial x_i}, \tag{9}$$

$$P_\omega = \alpha \frac{\omega}{k} P_k. \tag{10}$$

## 2.3. Numerical method

The system of governing equations (1)–(5) with appropriate boundary conditions has been successfully solved by using a numerical method, mainly based on the volume control approach (PATANKAR [19]). This method is based on the spatial integration of the conservation equations over finite control volumes. The numerical simulations were carried out with the ANSYS FLUENT® software. The convergence criteria were based on the residuals resulting from the integration of the conservation equations (1)–(5) over finite control volumes. During the iterative calculation process, these residuals were constantly monitored and carefully examined. For all the simulations performed in this study, converged solutions were usually achieved with residuals as low as $10^{-5}$ (or less) for all the governing equations.

# 3. Results and discussion

Wall shear stress and static pressure are fundamental parameters in high-level swimming. When a swimmer moves in aquatic environment, negative pressure gradients and turbulence zones are generated around his body (LYTTLE [20]) because of the non-uniformity and complexity of the human body. This particularly occurs in the areas where the body shape, globally rigid in form, presents complex surface geometries such as the head, shoulders, buttocks, heel and chest (CLARYS [21]). This may involve a boundary layer separation (figure 4) located in the concave geometries of the body (nape, chin and buttock). Figures 5 and 6 present the surface shear stress distribution on the swimmer's body for three positions of the head, namely lifted up (position 1), aligned (position 2) and lowered (position 3), in back and front views. Numerical results are provided for a high velocity ($U_0$ = 3.1 m/s) that corresponds to an international class swimmer. One may observe that the wall shear stress is higher behind the head for position 1 (figure 5(a)) and on the forehead in position 3 (figure 6(c)). Figures 7 and 8 show the back and front views of the pressure field for each of the three head positions and $U_0$ = 3.1 m/s. The negative pressure gradients may be observed behind the head for position 1 (figure 7(a)) and on the forehead in position 3 (figure 8(c)), which testifies to the separation zones in these areas. Moreover, it is found that the position of the head aligned with the body is the one that offers less resistance in underwater glide swimming in comparison with the positions of the head lifted up and lowered. A similar result was obtained by ZAÏDI et al. [15] in their 2D study.

Wall shear stress distributions on the swimmer's body (back and front views) for the position of the

Fig. 4. Back and front views of the streamline patterns around the swimmer in position 2 (head aligned with the body) and at $U_0 = 3.1$ m/s

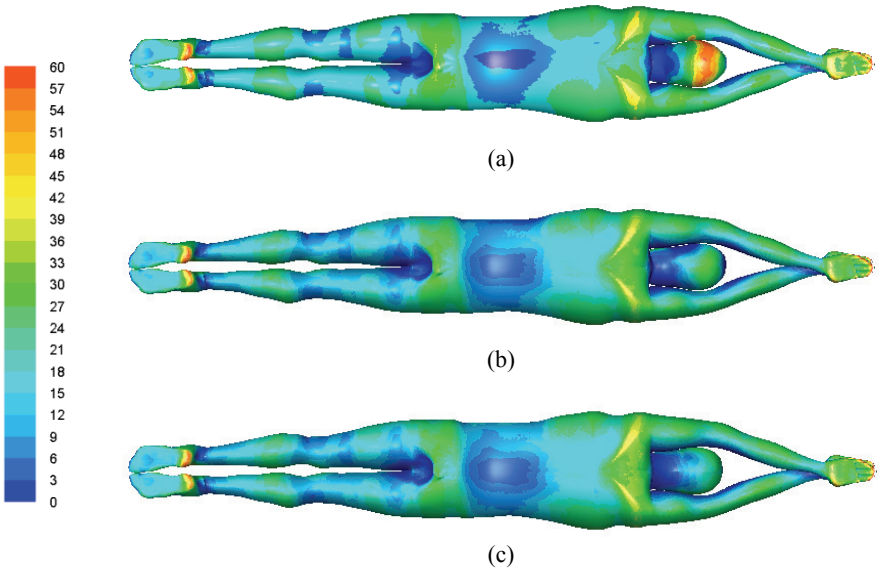


Fig. 5. Back views of the wall shear stress distribution on the swimmer at $U_0 = 3.1$ m/s and for three head positions: (a) lifted up, (b) aligned and (c) lowered

head aligned (position 2) and at three velocities ($U_0$ = 1.4, 2.2 and 3.1 m/s) are presented in figures 9 and 10. The pressure gradient between the different parts of the swimmer generates a drag force that acts perpendicular to the surface of the body and slows the movement of the swimmer (RUSHALL et al. [22]). The higher the drag force, the higher the wall shear stress observed. It is found that the wall shear stress increases with velocity, leading to an increased drag force. Wall shear stresses are also important in the

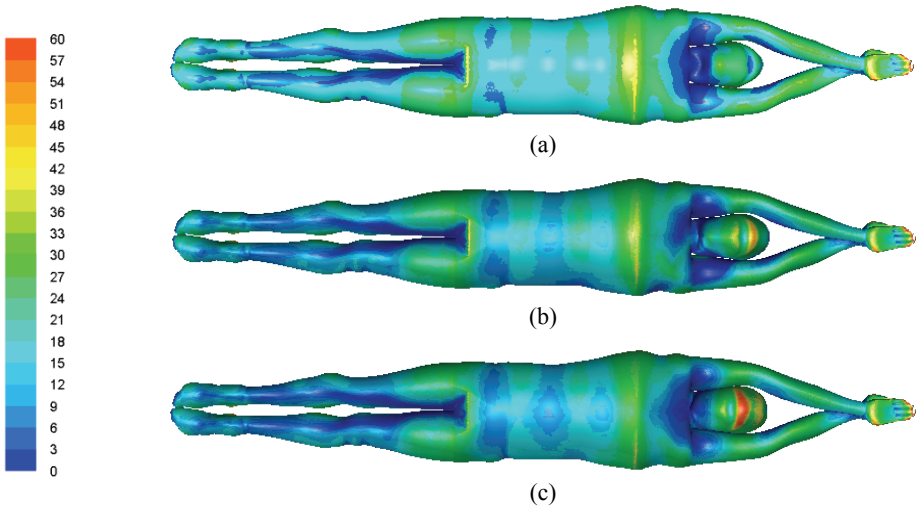


Fig. 6. Front views of the wall shear stress distribution on the swimmer at $U_0 = 3.1$ m/s and for three head positions: (a) lifted up, (b) aligned and (c) lowered

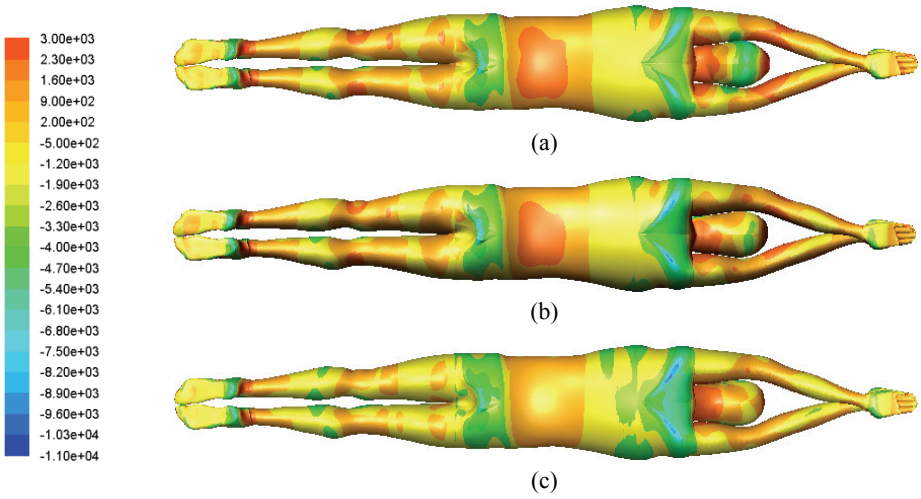


Fig. 7. Back views of the pressure field on the swimmer at $U_0 = 3.1$ m/s and for three head positions: (a) lifted up, (b) aligned and (c) lowered

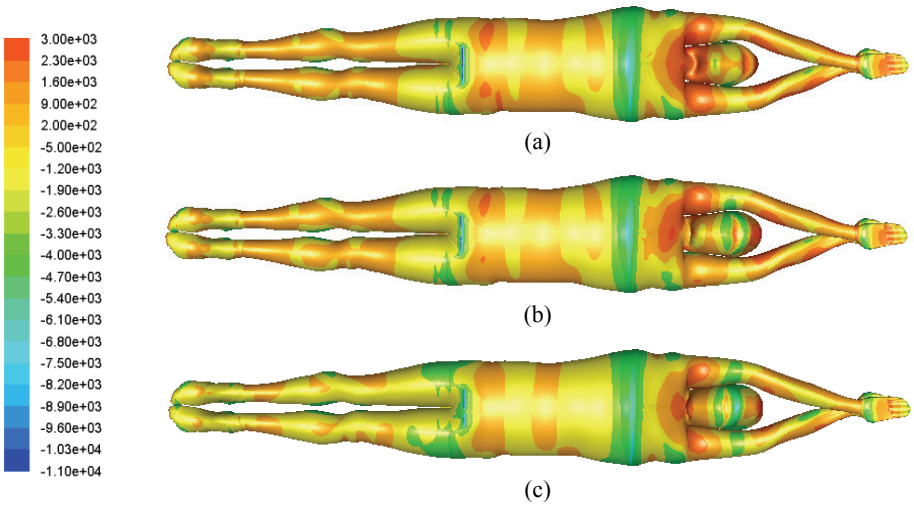


Fig. 8. Front views of the pressure field on the swimmer at $U_0 = 3.1$ m/s and for three head positions: (a) lifted up, (b) aligned and (c) lowered

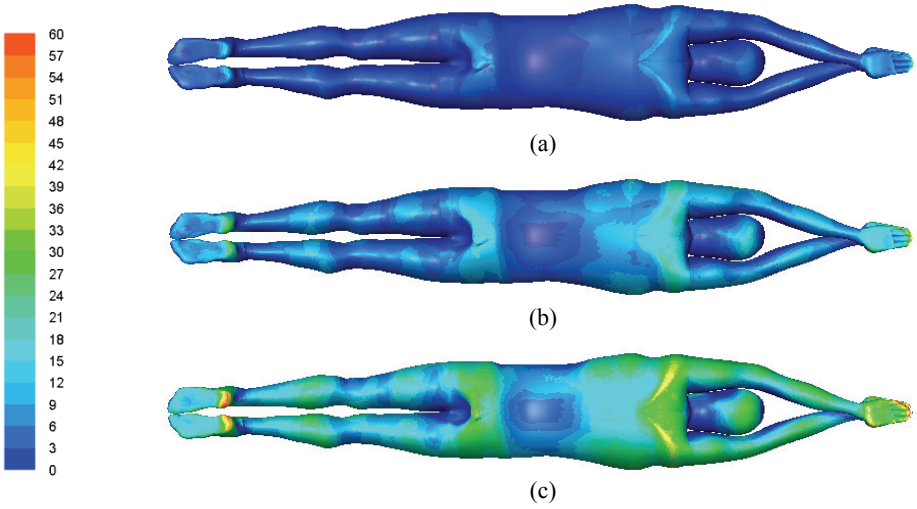


Fig. 9. Back views of the wall shear stress distribution on the swimmer in position 2, obtained at three velocities: (a) $U_0$ = 1.4 m/s, (b) $U_0$ = 2.2 m/s and (c) $U_0$ = 3.1 m/s

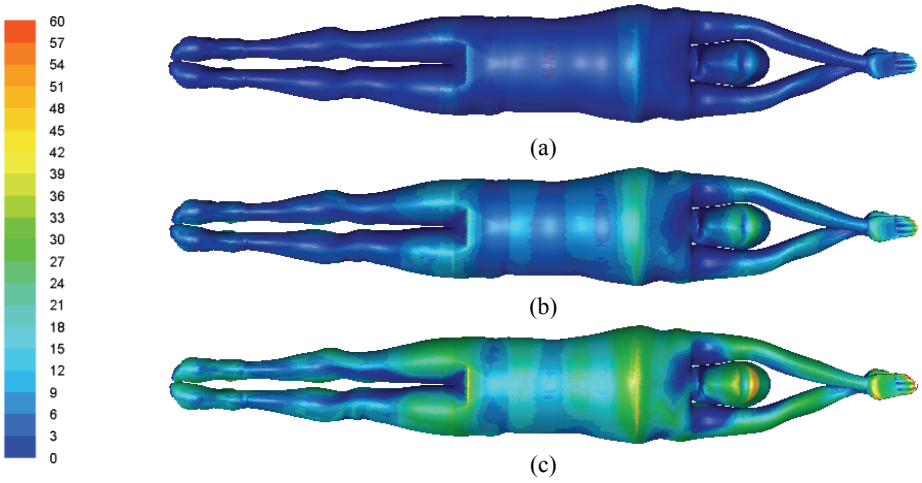


Fig. 10. Front views of the wall shear stress distribution on the swimmer in position 2, obtained at three velocities: (a) $U_0$ = 1.4 m/s, (b) $U_0$ = 2.2 m/s and (c) $U_0$ = 3.1 m/s

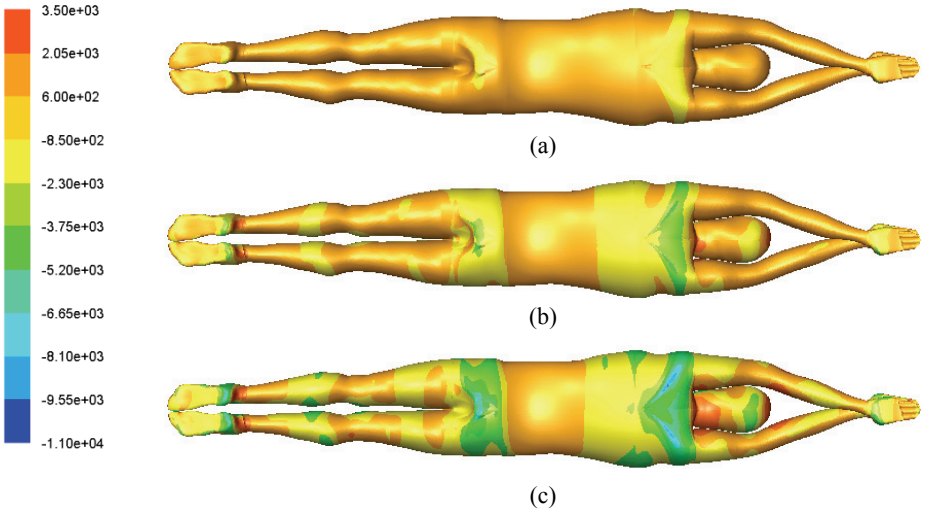


Fig. 11. Back views of the pressure field on the swimmer in position 2, obtained at three velocities: (a) $U_0$ = 1.4 m/s, (b) $U_0$ = 2.2 m/s and (c) $U_0$ = 3.1 m/s

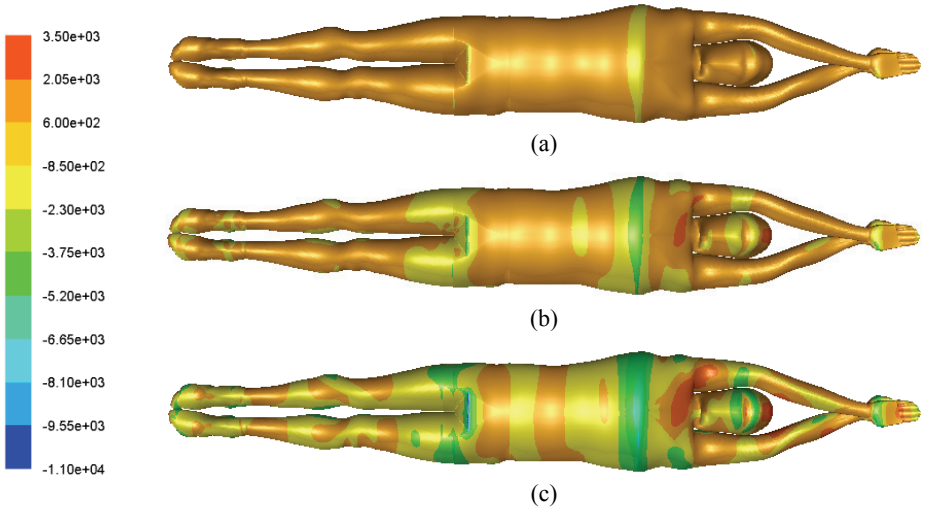


Fig. 12. Front views of the pressure field on the swimmer in position 2, obtained at three velocities: (a) $U_0$ = 1.4 m/s, (b) $U_0$ = 2.2 m/s and (c) $U_0$ = 3.1 m/s

areas where the body shape, globally rigid in form, presents complex surface geometries such as the head, shoulders, buttocks, heel and chest. In these regions, flow separations occur and the pressure decreases sharply. In particular, the areas with strong negative pressure gradients for $U_0$ = 3.1 m/s may be observed (figure 10). These areas correspond to zones where the boundary layer becomes separated which is in agreement with the numerical streamline field drawn in figure 4.

Figures 11 and 12 present, respectively, back and front views of the pressure field on the swimmer in position 2, obtained at three velocities ($U_0$ = 1.4, 2.2 and 3.1 m/s). The areas with negative and positive pressure gradients are clearly identified in these figures. Significant differences are observed between the front and back views of the swimmer. As far as velocities increase, the amplitudes of the positive and negative pressure gradients increase. In particular, one may observe the areas with strong negative pressure gradients at $U_0$ = 3.1 m/s, corresponding to zones where the flow is separated (figure 4).

# 4. Conclusion

The objective of this paper was to study the flow dynamics using a CFD code around a competitive swimmer during underwater glide swimming phase at three different velocities. The influence of the head position, namely lifted up, aligned and lowered, has been analyzed, taking account of the wall shear stress and static pressure. It may be observed that wall shear stresses are important in the areas where the body shape, globally rigid in form, presents complex surface geometries such as the head, shoulders, buttocks, heel and chest. In these regions, flow separations occur and the pressure decreases sharply. The wall shear stress is higher behind the head for position 1 and on the forehead in position 3 than for the other cases. Moreover, the wall shear stress increases with increasing velocity and the resistance force to moving ahead increases with the surface shear stress. The areas with negative and positive pressure gradients are clearly identified and significant differences are observed between the front and back views of the swimmer. As far as velocities increase, the amplitudes of the positive and negative pressure gradients also increase. The areas with strong negative gradients, corresponding to the zones where flow separations occur, are observed.

## References

[1] HUIJING P.A., TOUSSAINT H.M., CLARYS J.P., de GROOT G., HOLLANDER A.P., VERVOORN K., MACKAY R., SAVELBERG H.H.C.M., *Active drag related to body dimensions*, [in:] B.E. Ungerechts, K. Reischle, K. Wilke (Eds.), *In Swimming Science* V. *Human Kinetics Books*, Champaign, Ill, 1988, 31–37.

[2] KOLMOGOROV S.V., DUPLISHCHEVA O.A., *Active drag, useful mechanical power output and hydrodynamic force coefficient in different swimming strokes at maximal velocity*, Journal of Biomechanics, 1992, Vol. 25, 311–318.

[3] TOUSSAINT H.M., de GROOT G., SAVELBERG H.H.C.M., VERVOORN K., HOLLANDER A.P., van INGEN SCHENAU G.J., *Active drag related to velocity in male and female swimmers*, Journal of Biomechanics, 1988, Vol. 21, 435–438.

[4] TOUSSAINT H.M., ROOS P.E., KOLMOGOROV S., *The determination of drag in front crawl swimming*, Journal of Biomechanics, 2004, Vol. 37, 1655–1663.

[5] TOUSSAINT H.M., TRUIJENS M., *Biomechanical aspects of peak performance in human swimming*, Journal of Animal Biology, 2005, Vol. 25, 17–40.

[6] ADKINS D., YAN Y.Y., *CFD Simulation of fish-like body moving in viscous liquid*, Journal of Bionic Engineering, 2006, Vol. 3(3), 147–153.

[7] KATO N., AYERS J., MORIKAWA H., *Bio-mechanisms of Swimming and Flying*, Springer-Verlag, Tokyo, 2004.

[8] SATO Y., HINO T., *CFD simulation of flows around a swimmer in a prone glide position*, Japanese Journal of Sciences in Swimming and Water Exercise, 2010, Vol. 13, No. 1, 1–9.

[9] MARINHO D.A., BARBOSA T.M., KJENDLIE P.L., MANTRIPRAGADA N., VILAS-BOAS J.P., MACHADO L., ALVES F.B., ROUBOA A.I., SILVA A.J., *Modelling Hydrodynamic Drag in Swimming using Computational Fluid Dynamics*, *Computational Fluid Dynamics*, Hyoung Woo Oh (Ed.), 2010, InTech, Available from: http://www.intechopen.com/articles/show/title/modelling-hydrodynamic-drag-in-swimming-using-computational-fluid-dynamics.

[10] BIXLER B., RIEWALD S., *Analysis of swimmer's hand and arm in steady flow conditions using computational fluid dynamics*, Journal of Biomechanics, 2002, Vol. 35, 713–717.

[11] ROUBOA A., SILVA A., LEAL L., ROCHA J., ALVES F., *The effect of swimmer's hand/forearm acceleration on propulsive forces generation using computational fluid dynamics*, Journal of Biomechanics, 2006, Vol. 39, 1239–1248.

[12] GARDANO P., DABNICHKI P., *On hydrodynamics of drag and lift of the human arm*, Journal of Biomechanics, 2006, Vol. 39, 2767–2773.

[13] BIXLER B., PEASE D., FAIRHURST F., *The accuracy of computational fluid dynamics analysis of the passive drag of a male swimmer*, Sports Biomechanics, 2007, Vol. 6, 81–98.

[14] NAEMI R., EASSON W.J., SANDERS R.H., *Hydrodynamic glide efficiency in swimming*, Journal of Science and Medicine in Sport, 2010, 13(4), 444–451.

[15] ZAÏDI H., FOHANNO S., TAÏAR R., POLIDORI G., *Analysis of the effect of swimmer's head position on swimming performance using computational fluid dynamics*, Journal of Biomechanics, 2008, Vol. 41, 1350–1358.

[16] ZAÏDI H., TAÏAR R., FOHANNO S., POLIDORI G., *An evaluation of turbulence models in CFD simulations of underwater swimming*, Series on Biomechanics, 2009, Vol. 24, 1–5.

[17] ZAÏDI H., FOHANNO S., TAÏAR R., POLIDORI G., *Turbulence models choice for the calculating of drag forces when using CFD method*, Journal of Biomechanics, 2010, Vol. 43, 405–411.

[18] POLIDORI G., TAÏAR R., FOHANNO S., MAI T.H. LODINI A., *Skin-friction drag analysis from the forced convection modeling in simplified underwater swimming*, Journal of Biomechanics, 2006, Vol. 39, 2535–2541.

[19] PATANKAR S.V., *Numerical Heat Transfer and Fluid Flow*, Hemisphere, New York, 1980.

[20] LYTTLE A.D., *Hydrodynamics of the Human Body During the Freestyle Tumble Turn*, PhD Thesis, The University of Western Australia, Nedlands, Australia, 1999.

[21] CLARYS J.P., *Human morphology and hydrodynamics*, [in:] J. Terauds & E.W. Bedingfield (Eds.), *International Series on Sports Science* 8; *Swimming* III, 1979, 3–41. Baltimore, USA, University Park Press.

[22] RUSHALL B.S., HOLT L.E., SPRIGINGS E.J., CAPPAERT J.M., *A re-evaluation of forces in swimming*, Journal of Swimming Research, 1994, Vol. 10, 6–30.7